

ADVERSARIAL ROBUSTNESS THROUGH ARTIFACT DESIGN

Tsufit Shua*
Tel Aviv University

Mahmood Sharif†
Tel Aviv University

Abstract

Adversarial examples arose as a challenge for machine learning. To hinder them, most defenses alter how models are trained (e.g., adversarial training) or inference is made (e.g., randomized smoothing). Still, while these approaches markedly improve models’ adversarial robustness, models remain highly susceptible to adversarial examples. Identifying that, in certain domains such as traffic-sign recognition, objects are implemented per standards specifying how artifacts (e.g., signs) should be designed, we propose a novel approach for improving adversarial robustness. Specifically, we offer a method to redefine standards, making minor changes to existing ones, to defend against adversarial examples. We formulate the problem of artifact design as a robust optimization problem, and propose gradient-based and greedy search methods to solve it. We evaluated our approach in the domain of traffic-sign recognition, allowing it to alter traffic-sign pictograms (i.e., symbols within the signs) and their colors. We found that, combined with adversarial training, our approach led to up to 25.18% higher robust accuracy compared to state-of-the-art methods against two adversary types, while further increasing accuracy on benign inputs.

1. Introduction

Adversarial examples (Biggio et al., 2013; Szegedy et al., 2014)—mildly perturbed variants of benign samples crafted to mislead machine learning (ML) models at inference time—pose a risk to ML-based systems. For instance, adversarial examples were shown to mislead face recognition systems (Sharif et al., 2016), enabling adversaries to circumvent access-control and surveillance systems. As another example, adversarial examples were demonstrated to evade traffic-sign recognition (Eykholt et al., 2018), raising doubts about the safety of autonomous vehicles.

Varied defenses against adversarial examples have been pro-



Figure 1: Traffic signs with original pictograms and colors (top) vs. ones our method creates to defend against adversaries in the digital (middle) and physical (bottom) domains.

posed. Some defenses mainly intervene at training time, altering how models are trained. For instance, adversarial training augments training data with adversarial examples to improve models’ adversarial robustness (Goodfellow et al., 2015; Madry et al., 2018; Wu et al., 2020). Other defenses primarily intervene during inference. For example, randomized smoothing runs inference with multiple samples augmented with noise to approximate a model with increased robustness and derive provable robustness guarantees (Cohen et al., 2019; Carlini et al., 2023). While helpful at improving robustness, existing approaches have exhibited limited improvements on standard benchmarks in recent years, leading to calls for dramatically different methods for boosting adversarial robustness (Kolter, 2023).

This paper proposes such an approach, offering means to alter the underlying data distribution to improve models’ adversarial robustness. Our insight is that, in some domains such as traffic-sign and license-plate recognition (Maletzky et al., 2021; Wikipedia Contributors), artifacts whose samples are ingested as inputs are defined by human-created *standards* specifying how artifacts should be designed (see Def. 1). Take traffic signs, for instance—each sign is implemented according to a standard specifying how its external shape, pictogram (i.e., symbols within signs), and pictogram color should appear (see Fig. 1). Guided by this insight, we *explore means to apply minor changes to existing standards (e.g., so that humans would still be able to recognize traffic signs), redefining artifact designs, to enhance the adversarial robustness of models trained and evaluated on data generated according to the standards*.

*tsufitronen@mail.tau.ac.il

†mahmoods@tauex.tau.ac.il

We formalize the problem of artifact design as a robust optimization problem. The goal of the optimization is to find a standard specification and model that minimizes the maximum loss attainable by adding worst-case adversarial perturbations to artifacts designed per the standard. To solve the optimization, we offer two approaches. The first approach leverages gradient-based optimization to optimize artifact attributes differentiable with respect to the loss, such as traffic-sign colors. The second approach adopts greedy optimization to optimize discrete attributes, such as pictograms. We tested our approach in the traffic-sign domain under two commonly studied threat models (Fig. 1 depicts results). One threat model considers adversaries in the digital domain, adding adversarial perturbations bounded in ℓ_p -norm to evade classification (e.g., (Goodfellow et al., 2015)). In contrast, the other threat model considers physical domain adversaries introducing small, inconspicuous patches to inputs to mislead models (e.g., (Eykholt et al., 2018)). In both settings, our approach suggested traffic-sign pictograms and colors that significantly improved adversarial robustness compared to state-of-the-art methods (by up to 25.18% robust accuracy). As an added benefit, our approach also enhances models’ accuracy on benign inputs.

Next, we describe relevant background and related work (§2), and the threat model (§3). Then, we present our methods (§4) and results (§5–6) before concluding (§7).

2. Background and Related Work

2.1. Evasion Attacks

Various attack types against ML, varying in attackers’ goals and capabilities, exist. For example, in training-time attacks, adversaries harm model accuracy by partially controlling the training data or process (e.g., (Biggio & Roli, 2018; Huang et al., 2021)); in privacy attacks, adversaries extract private information about training data during or after training (e.g., (Shokri et al., 2017)); and, in availability attacks, adversaries generate inputs that increase prediction or training time (e.g., (Shumailov et al., 2021)). Unlike these, this work deals with *evasion attacks*, where adversaries can only manipulate inputs during inference to induce misclassifications.

Biggio et al. (2013) and Szegedy et al. (2014) first proposed evasion methods against ML models for image classification via *adversarial examples*. To generate adversarial examples, they proposed methods to find worst perturbations, with small ℓ_p -norm for imperceptibility, that increase models’ loss, thus leading to misclassification. Since then, many studies offered more successful, efficient, and imperceptible attacks (e.g., (Goodfellow et al., 2015; Carlini & Wagner, 2017; Papernot et al., 2017; Madry et al., 2018; Croce & Hein, 2020)). Typically, adversarial examples are generated

by solving an optimization of the form:

$$\operatorname{argmax}_{\delta} \mathcal{L}(\mathcal{F}(x + \delta_{adv}^x), y) \quad \text{s.t. } \|\delta_{adv}^x\|_p \leq \epsilon.$$

This optimization looks for the the adversarial perturbation (δ_{adv}^x) with bounded ℓ_p -norm (by ϵ), whose addition to the benign sample (x) misleads the model (\mathcal{F}), by increasing the loss (\mathcal{L}).

Adversaries vary, among others, in their abilities and goals (Papernot et al., 2016). In *white-box* settings (e.g., (Madry et al., 2018)), attackers have access to the model parameters and architectures. In contrast, in *black-box* settings (e.g., (Papernot et al., 2017)), attackers are only allowed to query models and have no access to their internals. Attacks may also target a particular class or seek an arbitrary misclassification (a.k.a. untargeted attacks) (Papernot et al., 2016). Intuitively, untargeted white-box attacks are most potent; thus, we primarily evaluate defenses’ robustness against such attacks (§3).

Adversarial perturbations bounded in ℓ_p -norm are well-suited for assessing robustness in the digital domain, where adversaries have complete control over inputs. Yet, as adversaries may have limited control over inputs in real-world scenarios (e.g., due to sampling noise), researchers also explored adversarial examples realizable in the physical domain (e.g., (Sharif et al., 2016; Brown et al., 2017; Athalye et al., 2018; Eykholt et al., 2018; Zha et al., 2020)). These attacks are usually implemented in the form of visible-yet-inconspicuous perturbations that are added to inputs (e.g., as stamps on traffic signs) to induce misclassification. In this work, we also seek to defend against such attacks (§3).

2.2. Defenses Against Evasion Attacks

Defending models against adversarial examples is a chief problem in adversarial ML. Adversarial training—augmenting the training data with correctly labeled adversarial examples—is of the most effective techniques for enhancing robustness (Goodfellow et al., 2015; Madry et al., 2018; Wu et al., 2020; Pang et al., 2022). Notably, Madry et al. (2018) framed the problem of training adversarially robust models as a robust optimization problem:

$$\min_{\mathcal{F}} \mathbb{E} \left[\max_{\delta_{adv}^x} \mathcal{L}(\mathcal{F}(x + \delta_{adv}^x), y) \right] \quad (1)$$

where the objective is to find a classifier (\mathcal{F}) whose expected maximum loss on adversarial examples is as low as possible. We offer a related formalism to design standards conducive for robustness (Eqn. 2 in §4).

Other defenses offer methods to detect adversarial inputs (Meng & Chen, 2017; Metzen et al., 2017), transform inputs prior to classification to sanitize adversarial perturbations (Samangouei et al., 2018; Xu et al., 2018), and certify

robustness within certain regions (e.g., by verifying that all samples in them are classified the same) (Cohen et al., 2019; Singh et al., 2019; Carlini et al., 2023). Still, despite remarkable advances in improving ML models’ adversarial robustness over the past few years, models remain highly vulnerable to evasion attacks (Kolter, 2023). Our work aims to further enhance models’ adversarial robustness, further closing the gap, via a novel technique.

Prior work mostly focused on offering alternative training and inference techniques to improve robustness. In contrast, we propose enhancing robustness by altering how artifacts are designed. Somewhat related to our work, Salman et al. (2021) proposed creating a single artifact that is classified correctly with high likelihood under varied imaging conditions that are not necessarily adversarial (e.g., rain and fog). Unlike our work, however, they did not consider defending against adversarial examples, and created individual objects (e.g., airplanes) instead of altering standards specifying how artifacts of all classes should be designed.

Several studies argue that data distribution is a crucial factor impacting adversarial robustness (Shafahi et al., 2019; Ilyas et al., 2019; Richardson & Weiss, 2021; Shamir et al., 2021). In line with these, we aim to change the data distribution in domains where doing so is possible (e.g., traffic-sign recognition) to facilitate adversarial robustness.

3. Threat Model

Our work seeks to develop a defense against adversaries perturbing inputs to induce misclassifications by deep neural networks (DNNs). The adversaries we consider cannot alter the DNN weights or training process, as in training-time attacks, but only have control over inputs ingested by deployed models. We evaluate our defense against worst-case adversaries, as is standard in the literature (Croce et al., 2020; Wu et al., 2020). In particular, to evaluate our defense, we consider adversaries with white-box access to DNNs aiming to mislead them in an untargeted manner. Intuitively, weaker adversaries with more constrained access, or with the objective of targeting a specific target class, would be less successful circumventing the defense.

We aim to defend against two types of commonly studied adversaries. In the *digital threat model* (Croce & Hein, 2020), \mathcal{T}_{dig} , we consider adversaries producing adversarial inputs by adding perturbations bounded in ℓ_p -norm to benign inputs. Chiefly, we focus on perturbations bounded in ℓ_∞ -norm, which are widely studied in the literature (Croce et al., 2020). In the *physical threat model* (Eykholt et al., 2018), \mathcal{T}_{phys} , we consider adversaries introducing adversarial patches covering a small area of the image (e.g., $\sim 5\%$ of pixels (Wu et al., 2020)) with pixel values ranging anywhere $\in [0, 1]$. We clarify that, per standard practice, we consider

defending against one adversary type at a time. While a few approaches for defending against varied adversary types concurrently exist (Maini et al., 2020), such defenses exhibit limited success, and, to our knowledge, no defense exists for defending models under \mathcal{T}_{dig} and \mathcal{T}_{phys} . We thus defer defending against both adversaries simultaneously to future work.

To deter attacks, we consider defenses that not only alter how models are trained to improve their adversarial robustness, but can also alter artifacts to prevent adversaries from carrying out successful attacks. In particular, the defender may alter how artifact designs are specified in standards to improve the model’s robustness once the artifacts are implemented. The changes to artifact designs the defender is allowed to make are not without constraints. For example, they may need to be sufficiently minor so that the resulting artifacts would be easily identified by human observers.

4. Technical Approach

We frame the problem of designing standards conducive for adversarial robustness as a robust optimization problem, similarly to Madry et al.’s adversarial training process (Madry et al., 2018) (Eqn. 1 in §2). However, while adversarial training seeks to find model weights that minimize loss against worst-case perturbations of benign samples, we also aim to find specifications of standards that minimize loss against such perturbations. In other words, we seek to discover ways to define how artifacts should be designed such that they would lend themselves to training models with higher adversarial robustness. Next, we provide definitions to help us formulate the robust optimization objective.

Definition 1 A standard \mathcal{S} specifying the design of n artifact classes is a set $\mathcal{S} = \{s_1, s_2, \dots, s_n\}$, s.t. each $s_i \in \mathcal{S}$ is a tuple specifying the design of artifacts in class y_i .

Conceptually, Def. 1 describes standards as sets specifying how artifacts of n classes should be implemented, where each tuple specifying an artifact class denotes the classes’ characteristics. Two canonical domains where standards often specify object designs are traffic-sign and license-plate recognition (Maletzky et al., 2021; Wikipedia Contributors). For instance, in the traffic-signs domain, s_i may specify the sign’s outer shape, where the shape can be circular for prohibitory signs or triangular for warnings; the pictogram, which is usually a symbol, picture, or number within the sign; and the pictogram’s color, which is typically black. As another example, standards for license plates may specify font types; font colors; spacing; and background colors.

Once defined, standards are usually fabricated (many times) into real-world artifacts, and these artifacts are placed within different environment. The artifacts are then sensed (e.g.,

photographed) under different environmental conditions (e.g., varied lighting and angles), resulting in data samples or instances. We capture this complex instantiation process of a standard by the instantiation operator:

Definition 2 $\mathcal{I}(\mathcal{S}) = \{x_1, x_2, \dots\}$ is an instantiation operator, mapping a standard \mathcal{S} to a set of instances, such that $\forall i, x_i \in [0, 1]^d$ (i.e., a d -dimensional vector).

Said differently, $\mathcal{I}(\mathcal{S})$ is the set reflecting the data distribution from which training and test samples are drawn. We reuse this notation to refer to instances pertaining to a single artifact class y_i by $\mathcal{I}(s_i)$.

Robust Optimization With these definitions, we can formulate the robust optimization for uncovering a standard \mathcal{S} conducive for adversarial robustness and an adversarially robust model \mathcal{F} by:

$$\min_{\mathcal{S}, \mathcal{F}} \mathbb{E}_{\substack{s_i \sim \mathcal{S} \\ x \sim \mathcal{I}(s_i)}} \left[\max_{\delta_{adv}^x} \mathcal{L}(\mathcal{F}(x + \delta_{adv}^x), y_i) \right]. \quad (2)$$

Put simply, this optimization aims to find the standard (\mathcal{S}) and model (\mathcal{F}) such that the worst-case adversarial perturbation (δ_{adv}^x) added to instances produced according to the standard would still result in low loss (\mathcal{L}), in expectation. Note that, we may also need to impose constraints on the standards that can be found by the optimization. For instance, in the traffic-sign domain, sign shapes have a particular meaning (e.g., triangles are used for warning), thus, they may not be changed. Additionally, we may want to specify standards that do not significantly deviate from widely used ones to ensure they remain human-interpretable.

To solve Eqn. 2, it is necessary to model the instantiation process captured by \mathcal{I} and to develop effective and efficient search techniques to optimize \mathcal{S} and \mathcal{F} . As aforementioned, we show how this can be done in the traffic-sign domain, as a case study. Because, in practice, instantiation is a complex and slow process (requiring artifact fabrication, placement, and sensing), we approximate it using efficient computational techniques (§4.1). We then present how to optimize traffic signs' colors and pictograms in standards to solve Eqn. 2 (§4.2)

4.1. Standard Instantiation

We estimate traffic-sign standard instantiation via a faithful synthesis approach proposed by Maletzky et al. (2021). Fig. 2 summarizes the complete synthesis process. To synthesize images, Maletzky et al. started with patches contain a prohibitory sign (round with red border) or a warning sign (triangular with red border), called *context scenes*, that were extracted from high-resolution photographs of traffic scenes on Austrian highways (①). Next, they replaced the pictograms in the context scenes by the pictograms of the

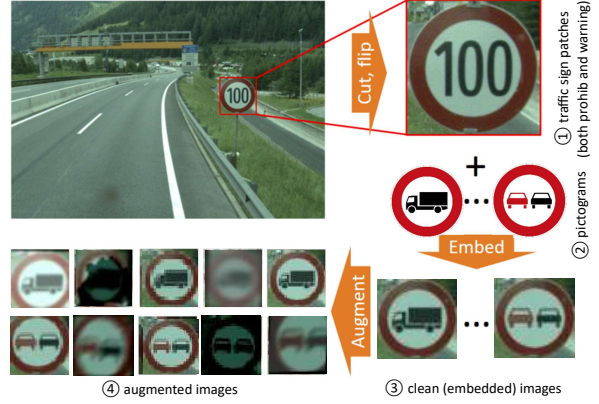


Figure 2: The dataset synthesis process used for standard instantiation, as presented by Maletzky et al. (2021).

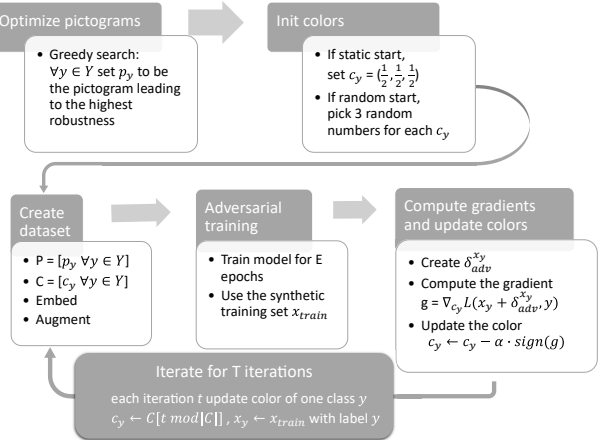


Figure 3: The standard-optimization process. After setting the pictograms via greedy optimization and the initial colors according to the selected initialization, we iteratively optimize the colors using gradient-based optimization.

traffic-sign classes (② and ③). Finally, they augmented the set of the images by applying an arsenal of augmentation methods with varying intensities, all selected at random (④). To enable gradient-based optimization of standards, it is necessary that all operations employed by the instantiation process would be differentiable. To this end, we ensured that all augmentation operations applied to instantiate images can be differentiated. We detail the augmentations' implementation and synthesis parameters when presenting the evaluation (§5.2).

4.2. Standard Optimization

We explore optimizing two characteristics of traffic signs to improve robustness—pictograms and their colors. Fig. 3 depicts the full optimization processes of both characteristics.

4.2.1. PICTOGRAM OPTIMIZATION

To optimize the pictograms, we leverage greedy discrete search. Given a pool of alternative pictograms per traffic-sign class, the search algorithm iterates over the traffic-sign classes one at a time, and chooses the pictogram leading to the highest robustness per class. We explored iterating over classes in a random order or starting with the classes exhibiting the lowest robust accuracy, and found the order had little-to-no impact on the results. More precisely, the pictogram optimization process works iteratively, as follows: (1) For the previously optimized classes, use the chosen pictogram with a black color (i.e. (0,0,0)); (2) for classes that have not yet been optimized, use the original pictogram with the original color; (3) instantiate different synthetic datasets, one per pictogram found in the search pool for the class currently being optimized; (4) adversarially train models on each of the datasets instantiated; (5) evaluate the robust accuracy of the models and select the pictogram corresponding to the model with the highest robust accuracy.

4.2.2. COLOR OPTIMIZATION

Color optimization leverages gradient-based search to search for solid pictogram colors conducive for robustness. Alg. 1 contains the pseudocode of the search process. The algorithm takes as input list of pictograms (P), potentially chosen by the pictogram-optimization process (§4.2.1), number of iterations (T), number of epochs (E) to (adversarially) train the model in each iteration, and a step size (α) for updating the pictogram colors in each iteration. Note that we found it is necessary to train the model simultaneously with optimizing colors, as, otherwise, the model would be most robust on the initial colors, and it would not be possible to further increase robustness by altering the colors alone.

Alg. 1 initializes pictogram colors by a static value (specifically, (0.5,0.5,0.5)) or by selecting a random color per pictogram (Line 3). The algorithm also initializes the model and selects an attack for generating potent adversarial examples per the adversary types (§3) it aims to defend against (Line 4). In each iteration, the algorithm updates the color of one class (Line 6), to ensure the optimization is stable (Zhu et al., 2019). The algorithm instantiates a synthetic dataset according to the pictograms P and the current colors C (Line 7), and trains the model for E epochs (Line 8), potentially via an adversarial training approach. Note that it is possible to set $E < 1$, whereby the model is trained only on part of the training data on each given iteration. Then, Alg. 1 generates adversarial perturbations for samples of the class selected for update during the iteration (Line 9). Next, it computes the gradient of the loss of the adversarial examples with respect to the pictogram’s color (Line 10). Notice that the gradients are computed over the worst-case inputs (i.e., adversarial examples), as is usually done in robust

Algorithm 1 Color Optimization

```

1: Input: Pictograms  $P$ , iters.  $T$ , epochs  $E$ , step size  $\alpha$ 
2: Output: Pictogram colors  $C$ 
3: Initialize  $C$                                       $\text{// } \text{len}(C) == \text{len}(P)$ 
4: Initialize  $\text{model}, \text{attack}$ 
5: for  $t \in T$  do
6:    $y \leftarrow t \bmod \text{len}(P)$ ,  $c_y \leftarrow C[y]$ 
7:    $x_{\text{train}} \leftarrow \text{CreateDataset}(P, C)$ 
8:    $\text{model}.train(x_{\text{train}}, \text{epochs} = E)$ 
9:    $\delta_{\text{adv}}^y \leftarrow \text{attack}.generate(x_{\text{train}}^y, y)$ 
10:   $g \leftarrow \nabla_{c_y} \mathcal{L}(x_{\text{train}}^y + \delta_{\text{adv}}^y)$ 
11:   $c_y \leftarrow c_y - \alpha \cdot \text{sign}(g)$ 
12:   $C[y] \leftarrow \text{clip}(c_y, 0, 1)$ 
13: end for
14: return  $C$ 

```

optimization (Madry et al., 2018). Finally, the algorithm updates the color in a direction opposite to the gradient, as to minimize the loss (Line 11), and clips the colors to ensure they remain valid (Line 12).

5. Experimental Setup

Here we discuss the setup used for our evaluation.

5.1. Models

The primary model architecture we employed is ResNet-18 (He et al., 2016), previously found to attain high performance on a standard traffic-sign recognition benchmark (Stallkamp et al., 2012; Moraes, 2018). Additionally, to demonstrate the generality of our findings, we tested models of two other popular architectures: MobileNet (Sandler et al., 2018) and VGG (Simonyan & Zisserman, 2015).

5.2. Dataset

As abovementioned (§4.1), we employed Maletzky et al.’s (2021) method to instantiate the dataset. We selected all pictograms implemented by Maletzky et al. that are also found in a standard traffic-sign dataset (Stallkamp et al., 2012), resulting in *seven* pictograms in total (② in Fig. 2). I.e., the models we trained aimed to distinguish between seven classes. To create images, the synthesis approach begins with 14 context scenes, into which pictograms are embedded: seven containing prohibitory signs (circle with red border) and seven containing warning signs (triangle with red border). These scenes are doubled in number by horizontal flipping (① in Fig. 2). The method then embeds each of the seven pictograms in the appropriate scenes, both original and flipped, generating an initial set of 98 images

of prohibitory and warning traffic-signs (③ in Fig. 2).

In the next stage, the synthesis method applies image augmentations to produce realistic traffic-sign images. Maletzky et al. used the `imgaug` Python package to implement augmentations (Jung et al., 2020). However, the transformations used for augmentation in this package are not differentiable, rendering them unsuitable for color optimization process, as discussed in §4.1. Thus, we implemented 15 augmentation methods (Gaussian noise, motion blurring, darken etc.) similar to those in Maletzky et al.’s using `kornia`’s differentiable operations (Riba et al., 2020).

For each of the 98 initial images, we generated 225 images, by applying a battery of up to eight randomly selected augmentations with varied intensities (④ in Fig. 2). Eventually, the dataset consisted of 22,050 images, equally distributed across source context scenes, classes, and augmentation methods. To evaluate the generalization of models, we held the images corresponding to two prohibitory-sign and two warning-sign context scenes for testing, while the remainder were used for training (96.7%) and validation (3.3%).

App. A qualitatively and quantitatively evaluates the instantiated dataset, demonstrating its qualities resemble those of a real traffic-sign dataset.

5.3. Attacks

To evaluate robustness under \mathcal{T}_{dig} , per standard practice, we used the AutoAttack (Croce & Hein, 2020)—an ensemble of four, advanced attacks, including two white-box attacks, and to black-box attacks. We limited the ℓ_∞ -norm of perturbations to $\epsilon = \frac{8}{255}$, as common (Croce et al., 2020).

In \mathcal{T}_{phys} , we assessed robustness using four attacks. Three of these attacks were previously established: (1) Brown et al.’s (2017) *adversarial patch* designs a position- and input-agnostic (universal) patch leading to misclassification to an *a priori* selected class; (2) Wu et al.’s (2020) *rectangular occlusion attack* (*ROA*) generates an image-specific adversarial noise, shaped as a square that is placed in a position most likely to produce misclassification; and (3) Eykholt et al.’s (2018) *Robust Physical Perturbations* (RP_2) posts adversarially crafted multiple black and white stickers on signs to induce misclassifications. Additionally, we considered RP_2^m —an attack we developed by combining elements of RP_2 and *ROA*. RP_2^m finds m square-shaped adversarial stickers via an optimization process similar to the RP_2 . App. B provides further details about RP_2^m and reports a comparison between them. We found that RP_2^4 outperformed all other attacks, thus we report models’ robust accuracy in \mathcal{T}_{phys} against it. In particular, we report results considering stickers covering $\sim 5\%$ of pixels in the image, a setting that is commonly studied (Wu et al., 2020). Fig. 9 in App. B depicts attack examples.

5.4. Adversarial Training

We considered two adversarial training approaches as baselines that we later integrated into our standard-optimization approach. To select these defenses, we searched for top-performing adversarial training techniques that do *not* rely on external unlabeled data and have open-source implementations. Following this criteria, for \mathcal{T}_{dig} , we used the *SCORE* adversarial training technique (Pang et al., 2022), which ranks amongst the leading defenses on the Robust-Bench benchmark (Croce et al., 2020). For \mathcal{T}_{phys} , we used *Defense against Occlusion Attacks* (*DOA*) (Wu et al., 2020), a method performing adversarial training using adversarial examples created by *ROA*. App. C details the configurations of the two training methods.

5.5. Standard Optimization

Pictogram Optimization For each traffic-sign class, we collected five alternative pictograms for pictogram optimization via Internet search (e.g., by looking for terms such as “bike silhouette”). Fig. 10 in App. D presents the pictograms. To address certain inconsistencies observed in the adversarial training methods, we adversarially trained five models for each alternative pictogram, using a different randomness seed in each run, and selected the pictogram with the highest mean validation robust accuracy.

Color Optimization For each threat model, we performed a line search to find the parameters (i.e., iterations, epochs, and step size) for Alg. 1 that yield the highest robust accuracy. In \mathcal{T}_{dig} , we ran 600 iterations of Alg. 1, where, in each iteration, we adversarially trained the model for 0.5 epoch (i.e., trained one epoch using 0.5 of the training data) and updated the pictogram’s color by a step size of 0.01. Note that due to run-time limitations, in each iteration we ran 100 iterations of APGD-CE (one of the attacks employed by AutoAttack) (Croce & Hein, 2020) to produce adversarial examples (Line 9 of Alg. 1), instead of the complete AutoAttack, which was left for the evaluation (§5.3). In \mathcal{T}_{phys} , we ran 400 iterations of the algorithm with 0.25 training epochs per iteration, and a color update step-size of 0.01.

Because the dataset generation process is randomized and Alg. 1 is stochastic, solving a highly non-convex optimization, results could vary across runs. Thus, to enhance the reliability of the evaluation, we repeated each experiment with Alg. 1 ten times, each with a randomly instantiated dataset, using a different randomness seed in each run. We report the performance of the model corresponding to the highest validation robust accuracy.

6. Experimental Results

Our experiments answered several research questions: *RQ1*: To what extent does standard optimization improve robust

accuracy? (§6.1); *RQ2*: Does adversarially training models on the resulting standard from scratch yield equally robust models? (§6.2); *RQ3*: Which is more effective, color or pictogram optimization? (§6.3); *RQ4*: How does standard optimization compare to simpler means of designing standards? (§6.3); *RQ5*: Is standard optimization effective with varied model architectures? (§6.4). We present the experiment results in the following sections, demonstrating how standard optimization aids in improving adversarial robustness. We also report run times in App. E. Unless otherwise noted, the experiments report the performance of the complete standard-optimization process, executing color optimization after setting the pictograms to those found via the pictogram optimization process.

6.1. Defense Performance (*RQ1*)

To evaluate standard optimization, we started by measuring the benign and robust accuracy of models adversarially trained on the original pictograms and colors. Then, we gradually increased the number of traffic signs whose pictograms and colors are optimized using our approach. Fig. 4 presents the results, considering colors initialized at random or to fixed values. Compared to the adversarial training, the standard optimization with random initialization improved robust accuracy by 25.18% under \mathcal{T}_{dig} , and by 16.33% under \mathcal{T}_{phys} . An improvement of 1.30–5.63% was also attained for benign accuracy. These results evidence that standard optimization facilitates adversarial robustness. (The optimized standards are shown in Fig. 1.) Since the random initialization obtained comparable or better performance than static initialization in most cases, we report performance using random initialization in the following experiments.

6.2. Training From Scratch (*RQ2*)

In addition to the new standard, the optimization process produces a model that is optimized simultaneously with the standard. It remains unclear, however, whether (adversarially) training models from scratch on the resulting standard would result in models that have comparable benign and robust accuracy to those trained concurrently with standard optimization. To answer this question, we adversarially trained models on datasets instantiated per standards found by running the optimization with a varied number of pictograms. Fig. 5 presents the results. For \mathcal{T}_{dig} , the gap between the robust accuracy of the models trained from scratch and those obtained from the optimization process was small ($\pm 3\%$). For \mathcal{T}_{phys} , a little less consistency was observed, mostly due to large variance in robust accuracy when running vanilla adversarial training. Still, when all pictograms labels were optimized, the gap remained as small as 1.66%. Hence, we conclude that the results of the standard optimization process can be reproduced by adversarially training models from scratch using the optimized standard.

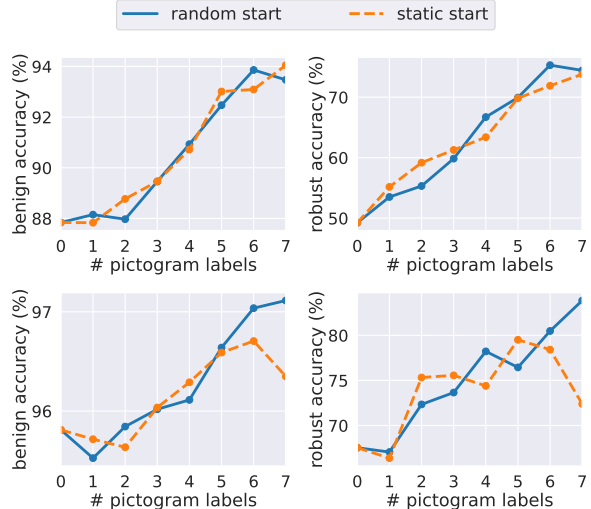


Figure 4: Benign and robust accuracy attained by standard optimization, with random and static initialization, while increasing the number of pictogram labels optimized, under both \mathcal{T}_{dig} (top) and \mathcal{T}_{phys} (bottom). Number of pictograms labels =0, corresponds to adversarial training.

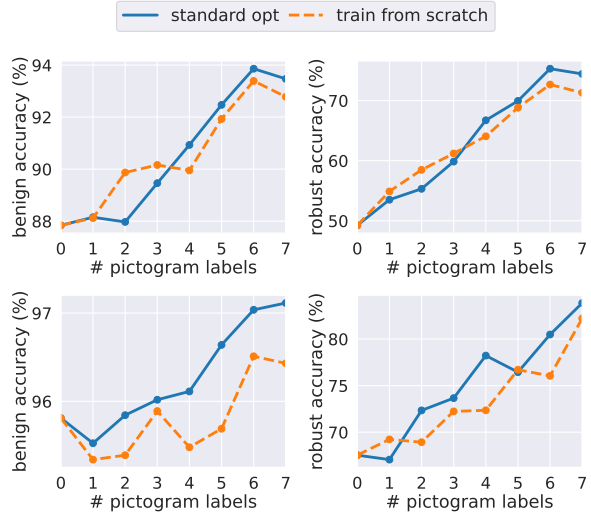


Figure 5: Benign and robust accuracy when training models throughout standard optimization vs. adversarially training models from scratch using the optimized standards, under both \mathcal{T}_{dig} (top) and \mathcal{T}_{phys} (bottom).

6.3. Baseline Comparisons and Ablation (*RQ3 & RQ4*)

The standard-optimization process alters both the pictograms and pictogram colors of traffic signs. To find which of these is more conducive for robustness, we compared the full standard-optimization process with pictogram optimization alone, where colors are set to default ones (i.e., black or black and red, depending on the sign). Additionally, we

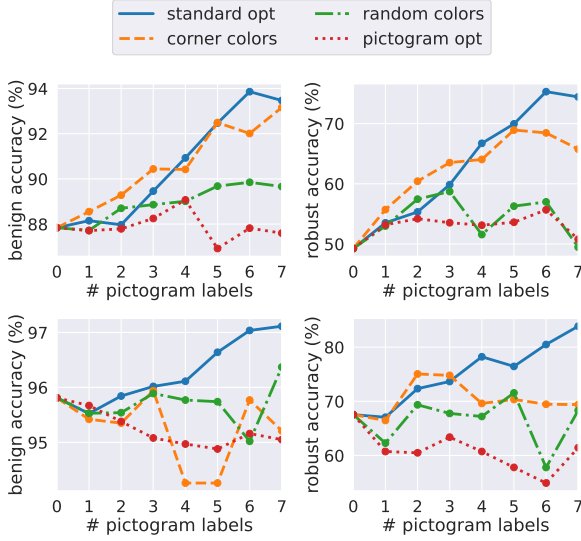


Figure 6: Test benign and robust accuracy of standard optimization compared to pictogram optimization alone and setting pictogram colors at random or to corner colors, under both \mathcal{T}_{dig} (top) and \mathcal{T}_{phys} (bottom).

wanted to assess the utility in optimizing pictogram colors via gradient-based optimization compared to less elaborate approaches. To this end, we considered two baselines. The first baseline sets the pictogram colors at random, by uniformly sampling them from the RGB color space. The second baseline is motivated by the observation that the color-optimization process finds colors close to the corners of the RGB color space excluding white color (i.e. to the colors in the group $C = \{c \in \{0, 1\}^3 : c \neq (1, 1, 1)\}$). Intuitively, we expected that maximizing the distance between the colors of different traffic-sign classes would enable distinguishing them more successfully. Thus, in the second baseline, we set pictogram colors by randomly permuting the seven possible values in C .

The results (Fig. 6) demonstrate that color optimization is more helpful than pictogram optimization for adversarial robustness, leading to $>20\%$ robust accuracy. Moreover, optimizing pictogram colors led to markedly higher robustness than the baselines: Both setting colors at random and selecting distinct corner colors for pictograms led to lower robust accuracy than pictogram optimization when optimizing the colors of all seven pictograms. These results demonstrate the utility of the standard-optimization process, and particularly that of color optimization.

6.4. Generality Across Architectures (RQ5)

Finally, we tested whether our results generalize across architectures. Here, we evaluated standard optimization on two architectures other than ResNet: MobileNet and VGG.

Table 1: Benign and robust accuracy of models adversarially trained and tested using the original standards, and on optimized standards, using different architectures.

(a) \mathcal{T}_{dig}			
Architecture	Dataset	Benign Acc.	Robust Acc.
ResNet	Original	87.84%	49.25%
	Optimized	93.47%	74.43%
MobileNet	Original	77.29%	28.09%
	Optimized	89.33%	60.58%
VGG	Original	87.98%	48.55%
	Optimized	93.34%	73.88%

(b) \mathcal{T}_{phys}			
Architecture	Dataset	Benign Acc.	Robust Acc.
ResNet	Original	95.81%	67.53%
	Optimized	97.11%	83.86%
MobileNet	Original	92.50%	45.28%
	Optimized	95.58%	69.86%

Using these architectures, we ran the optimization for all seven classes, and assessed both benign and robust accuracy under \mathcal{T}_{dig} and \mathcal{T}_{phys} , comparing them with the performance obtained via adversarial training on the original standard. Unfortunately, adversarial training using the original standard failed on the VGG models under \mathcal{T}_{phys} . Thus, we did not evaluate VGG under \mathcal{T}_{phys} . As shown in Tab. 1, our findings generalize across architectures—standard optimization consistently obtained higher benign and robust accuracy than adversarial training on all architectures and under both threat models.

7. Conclusion

We proposed a novel approach for hindering adversarial examples, suitable for domains where standards specify the designs of artifacts. Our approach slightly alters standards, re-specifying how artifacts should be designed to enhance adversarial robustness. We framed the problem of artifact design as a robust optimization, proposed gradient-based and greedy methods to solve it, and evaluated its viability in the traffic-sign domain against two well-studied attack categories. The results demonstrate significant improvements compared to state-of-the-art defenses (with up to 25.18% higher robust accuracy attainable via artifact design).

Acknowledgments

We would like to thank the PLUS research group’s members for their constructive feedback, and Maletzky et al. (2021) for sharing their implementation. This work was supported in part by a grant from the Blavatnik Interdisciplinary Cyber Research Center (ICRC); by Intel® via a Rising Star Faculty Award; by a gift from KDDI Research; by Len Blavatnik and the Blavatnik Family foundation; by a Maof prize for outstanding young scientists; by the Ministry of Innovation, Science & Technology, Israel (grant number 0603870071); by a gift from the Neubauer Family foundation; by NVIDIA via a hardware grant; by a scholarship from the the Shlomo Shmeltzer Institute for Smart Transportation at Tel Aviv University; and by a grant from the Tel Aviv University Center for AI and Data Science (TAD).

Impact Statements

This paper presents work whose goal is to advance the field of Machine Learning. There are many potential societal consequences of our work, none which we feel must be specifically highlighted here.

References

Athalye, A., Engstrom, L., Ilyas, A., and Kwok, K. Synthesizing robust adversarial examples. In *ICML*, 2018.

Biggio, B. and Roli, F. Wild patterns: Ten years after the rise of adversarial machine learning. In *CCS*, 2018.

Biggio, B., Corona, I., Maiorca, D., Nelson, B., Šrndić, N., Laskov, P., Giacinto, G., and Roli, F. Evasion attacks against machine learning at test time. In *ECML PKDD*, 2013.

Brown, T. B., Mané, D., Roy, A., Abadi, M., and Gilmer, J. Adversarial patch. *arXiv preprint*, 2017.

Carlini, N. and Wagner, D. Towards evaluating the robustness of neural networks. In *S&P*, 2017.

Carlini, N., Tramer, F., Dvijotham, K. D., Rice, L., Sun, M., and Kolter, J. Z. (Certified!!) adversarial robustness for free! In *ICLR*, 2023.

Cohen, J., Rosenfeld, E., and Kolter, Z. Certified adversarial robustness via randomized smoothing. In *ICML*, 2019.

Croce, F. and Hein, M. Reliable evaluation of adversarial robustness with an ensemble of diverse parameter-free attacks. In *ICML*, 2020.

Croce, F., Andriushchenko, M., Sehwag, V., Debenedetti, E., Flammarion, N., Chiang, M., Mittal, P., and Hein, M. Robustbench: A standardized adversarial robustness benchmark. *arXiv preprint*, 2020.

Eykholz, K., Evtimov, I., Fernandes, E., Li, B., Rahmati, A., Xiao, C., Prakash, A., Kohno, T., and Song, D. Robust physical-world attacks on deep learning visual classification. In *CVPR*, 2018.

Goodfellow, I. J., Shlens, J., and Szegedy, C. Explaining and harnessing adversarial examples. In *ICLR*, 2015.

He, K., Zhang, X., Ren, S., and Sun, J. Deep residual learning for image recognition. In *CVPR*, 2016.

Huang, H., Mu, J., Gong, N. Z., Li, Q., Liu, B., and Xu, M. Data poisoning attacks to deep learning based recommender systems. In *NDSS*, 2021.

Ilyas, A., Santurkar, S., Tsipras, D., Engstrom, L., Tran, B., and Madry, A. Adversarial examples are not bugs, they are features. *NeurIPS*, 2019.

Jung, A. B., Wada, K., Crall, J., Tanaka, S., Graving, J., Reinders, C., Yadav, S., Banerjee, J., Vecsei, G., Kraft, A., Rui, Z., Borovec, J., Vallentin, C., Zhydenko, S., Pfeiffer, K., Cook, B., Fernández, I., De Rainville, F.-M., Weng, C.-H., Ayala-Acevedo, A., Meudec, R., Laporte, M., et al. imgaug. <https://github.com/aleju/imgaug>, 2020. Last accessed on 2024-02-01.

Kolter, Z. Robustness in machine learning: A five-year retrospective. <http://tinyurl.com/SaTMLKeynoteKolter>, 2023. SaTML Keynote; last accessed on 2024-02-01.

Madry, A., Makelov, A., Schmidt, L., Tsipras, D., and Vladu, A. Towards deep learning models resistant to adversarial attacks. In *ICLR*, 2018.

Maini, P., Wong, E., and Kolter, Z. Adversarial robustness against the union of multiple perturbation models. In *ICML*, 2020.

Maletzky, A., Thumfart, S., and Wruß, C. An evaluation of the machine readability of traffic sign pictograms using synthetic data sets. *Verlag der Technischen Universität Graz*, 2021.

Meng, D. and Chen, H. Magnet: A two-pronged defense against adversarial examples. In *CCS*, 2017.

Metzen, J. H., Genewein, T., Fischer, V., and Bischoff, B. On detecting adversarial perturbations. In *ICLR*, 2017.

Moraes, R. GTSRB ResNet. https://github.com/mmoraes-rafael/gtsrb_resnet, 2018. Last accessed on 2024-02-01.

Nesterov, Y. A method for solving the convex programming problem with convergence rate $o(1/k^2)$. In *USSR Academy of Sciences*, 1983.

Pang, T., Lin, M., Yang, X., Zhu, J., and Yan, S. Robustness and accuracy could be reconcilable by (proper) definition. In *ICML*, 2022.

Papernot, N., McDaniel, P., Jha, S., Fredrikson, M., Celik, Z. B., and Swami, A. The limitations of deep learning in adversarial settings. In *Euro S&P*, 2016.

Papernot, N., McDaniel, P., Goodfellow, I., Jha, S., Celik, Z. B., and Swami, A. Practical black-box attacks against machine learning. In *ASIA CCS*, 2017.

Riba, E., Mishkin, D., Ponsa, D., Rublee, E., and Bradski, G. Kornia: An open source differentiable computer vision library for pytorch. In *WACV*, 2020.

Richardson, E. and Weiss, Y. A bayes-optimal view on adversarial examples. *The Journal of Machine Learning Research (JMLR)*, 22(1):10076–10103, 2021.

Salman, H., Ilyas, A., Engstrom, L., Vemprala, S., Madry, A., and Kapoor, A. Unadversarial examples: Designing objects for robust vision. *NeurIPS*, 2021.

Samangouei, P., Kabkab, M., and Chellappa, R. DefenseGAN: Protecting classifiers against adversarial attacks using generative models. In *ICLR*, 2018.

Sandler, M., Howard, A., Zhu, M., Zhmoginov, A., and Chen, L.-C. MobileNetV2: Inverted residuals and linear bottlenecks. In *CVPR*, 2018.

Shafahi, A., Huang, W. R., Studer, C., Feizi, S., and Goldstein, T. Are adversarial examples inevitable? In *ICLR*, 2019.

Shamir, A., Melamed, O., and BenShmuel, O. The dimpled manifold model of adversarial examples in machine learning. *arXiv preprint*, 2021.

Sharif, M., Bhagavatula, S., Bauer, L., and Reiter, M. K. Accessorize to a crime: Real and stealthy attacks on state-of-the-art face recognition. In *CCS*, 2016.

Shokri, R., Stronati, M., Song, C., and Shmatikov, V. Membership inference attacks against machine learning models. In *S&P*, 2017.

Shumailov, I., Zhao, Y., Bates, D., Papernot, N., Mullins, R., and Anderson, R. Sponge examples: Energy-latency attacks on neural networks. In *Euro S&P*, 2021.

Simonyan, K. and Zisserman, A. Very deep convolutional networks for large-scale image recognition. In *ICLR*, 2015.

Singh, G., Gehr, T., Püschel, M., and Vechev, M. An abstract domain for certifying neural networks. *PACMPL*, 2019.

Smith, L. N. and Topin, N. Super-convergence: Very fast training of neural networks using large learning rates. *arXiv preprint*, 2018.

Stallkamp, J., Schlipsing, M., Salmen, J., and Igel, C. Man vs. computer: Benchmarking machine learning algorithms for traffic sign recognition. *Neural Networks*, 2012.

Szegedy, C., Zaremba, W., Sutskever, I., Bruna, J., Erhan, D., Goodfellow, I., and Fergus, R. Intriguing properties of neural networks. In *ICLR*, 2014.

Wikipedia Contributors. United states license plate designs and serial formats. <http://tinyurl.com/LicensePlatesWiki>. Last accessed on 2024-02-01.

Wu, T., Tong, L., and Vorobeychik, Y. Defending against physically realizable attacks on image classification. In *ICLR*, 2020.

Xu, W., Evans, D., and Qi, Y. Feature squeezing: Detecting adversarial examples in deep neural networks. In *NDSS*, 2018.

Zha, M., Meng, G., Lin, C., Zhou, Z., and Chen, K. RoLMA: A practical adversarial attack against deep learning-based lpr systems. In *Inscrypt*, 2020.

Zhu, L., Liu, Z., and Han, S. Deep leakage from gradients. *NeurIPS*, 2019.

A. Evaluating Standard Instantiation

We wanted our synthesized dataset to resemble real traffic-sign datasets. Hence, we used the German Traffic Sign Recognition Dataset (GTSRB) (Stallkamp et al., 2012), a standard benchmark containing 48×48 images as a reference, leveraging it to qualitatively and quantitatively assess the similarity between our synthetically instantiated data and real data. To this end, we used all GTSRB samples from the same seven classes included in the synthesized dataset (§5.2).

To qualitatively assess the samples instantiated via synthesis, we visually compared them with images from GTSRB. Fig. 7 presents samples from synthetic dataset and GTSRB. It can be seen that the images from the GTSRB dataset and synthesized samples highly resemble one another, and can be hardly differentiated.



Figure 7: Examples from the synthetic dataset (top) vs. examples from the corresponding GTSRB classes (bottom).

Besides the qualitative assessment, we quantitatively measured the resemblance between our synthesized dataset and GTSRB by training models on one dataset and evaluating them on the other. Tab. 2 summarizes the results. It can be seen that the benign accuracy of the model trained and tested with the synthetic dataset is only slightly lower ($\sim 4\%$) than that of the model trained and tested using samples from the corresponding seven classes of GTSRB. For the models trained on the synthetic dataset using an adversarial training (both \mathcal{T}_{dig} and \mathcal{T}_{phys}), the benign accuracy when tested with the synthetic dataset is close to that of the standard training ($\pm 7\%$). The above three models trained on the synthetic dataset lose (as expected) up to 14% of the benign accuracy when tested on GTSRB. In general, it can be concluded that the synthetic dataset shows qualities similar to GTSRB’s. Accordingly, we expect that the findings on our datasets would generalize to real-world examples.

Table 2: Comparison between benign accuracy of a model trained and tested on GTSRB and models trained (via standard and adversarial training) on the synthetic dataset and tested with the synthetic dataset and GTSRB.

Training Dataset	Training Method	Test Dataset	
		Synthetic	GTSRB
GTSRB	Standard	—	97.18%
Synthetic	Standard	93.31%	79.49%
	Adv. \mathcal{T}_{dig}	86.49%	73.47%
	Adv. \mathcal{T}_{phys}	95.81%	93.38%

B. Attacks in \mathcal{T}_{phys}

As the implementation of the process finding sticker locations in Eykholt et al.’s attack is not publicly available, we used the fixed locations published by the authors for a particular traffic-sign class (specifically, stop signs). Unfortunately, however, this resulted in poor attack success rates. Thus, we combined elements of RP_2 and ROA to produce a more potent attack we denote by RP_2^m . Similarly to RP_2 , RP_2^m produces multiple stickers. Specifically, it finds m square-shaped stickers, each positioned at a location maximizing the loss during initialization (to a fixed color), as found by the exhaustive-search approach employed by ROA ((Wu et al., 2020)). Once the locations are set, the attack optimizes the sticker colors in the same manner as the RP_2 , while relaxing the constraint that each sticker is black and white.

Fig. 8 compares the three attacks (excluding Eykholt et al.’s due to its poor success rates), using the implementations published by Wu et al. (2020) for prior attacks. For ROA , we tested the slower but more successful variant, using exhaustive search to position the adversarial patch at a location that maximizes the loss the most. We ran the evaluation against a model defended via DOA (§5.4)—a state-of-the-art defense against physically realizable attacks—considering stickers of varied

sizes and different values of m in RP_2^m . It can be immediately seen that RP_2^4 consistently outperformed all other attacks and attack configurations. Therefore, we used RP_2^4 to assess the robustness of models we trained after standard optimization. In particular, in our evaluation, we report results considering stickers covering $\sim 5\%$ of pixels in the image, a setting that is commonly studied (Wu et al., 2020). Fig. 9 depicts attack examples.

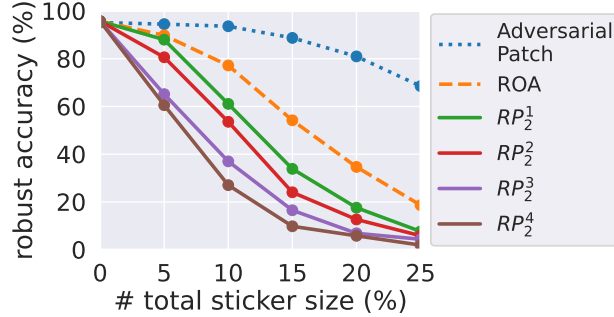


Figure 8: The robust accuracy of a model trained via *DOA* against different attacks under \mathcal{T}_{phys} , as a function of the total stickers size relative to the input image.

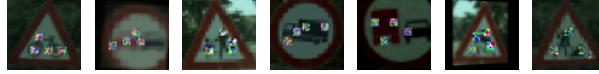


Figure 9: Examples of the RP_2^4 attack, with stickers covering $\sim 5\%$ of the image.

We clarify that, in our evaluation, we only considered digital representations of the physically realizable attacks. As physically implementing the attacks would likely be affected by implementation errors and sampling noise, our reported robust accuracy sets a lower bound on the actual robust accuracy attained against attacks implemented in the physical domain.

C. Adversarial Training Configurations

We tuned the adversarial training methods' parameters for best performance. For *SCORE*, per the original work, we used a batch size of 512 and trained the model for 400 epochs using the SGD optimizer with Nesterov momentum (Nesterov, 1983) (with a momentum factor of 0.9 and weight decay 5×10^{-4}). We further used the cyclic learning rate policy (Smith & Topin, 2018), with cosine annealing of the learning rate from an initial learning rate of 0.025 to maximum value of 0.01 and then to minimal value of $2.5e^{-6}$.

For *DOA*, following the original work, we first ran 30 epochs of standard training, using the SGD optimizer with initial learning rate of 0.03 and a step learning-rate scheduler decaying the learning rate by a factor of 0.1 every 15 epochs. Subsequently, we adversarially trained the model for additional 100 epochs, using the Adam optimizer and *SCORE*'s cyclic learning-rate scheduler. Similarly to the attack phase (§5.3), also in the training, we used a sticker of size covering $\sim 5\%$ of the image's pixels.

D. Pictogram Search-Space

Fig. 10 presents the original pictograms as well as the pictograms included in the search space for pictogram optimization.

E. Run-Time Measurements

To measure run times, we ran adversarial training and standard optimization on a single GPU—once on an NVIDIA A5000 and once on NVIDIA GeForce RTX 3090. The average run time of the adversarial training was 1.25 hours in \mathcal{T}_{dig} , and 8.17 hours in \mathcal{T}_{phys} . Standard optimization, which includes adversarial model training as part of the process (recall Alg. 1), took longer to run, but still completed in manageable time, requiring 28.92 hours in \mathcal{T}_{dig} and 22.83 in \mathcal{T}_{phys} . We highlight,

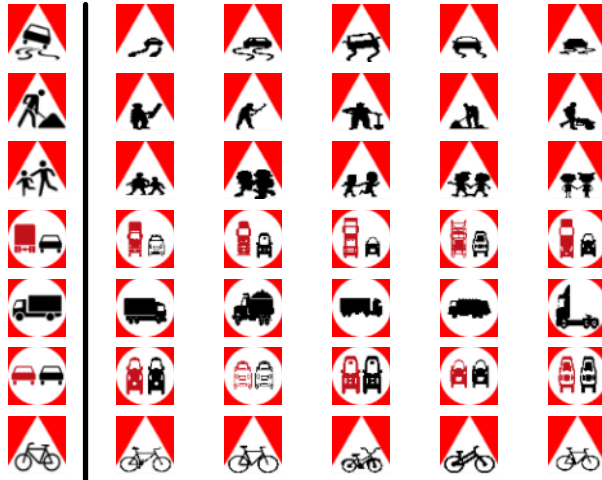


Figure 10: Original pictograms (leftmost column) and the alternatives used in pictogram optimization.

however, that we have not taken particular measures to optimize the time efficiency of standard optimization, and thus expect that it would be possible to markedly improve the run time. Furthermore, we note that, as highlighted by our evaluation (§6.2), once a standard conducive for adversarial robustness is found, it is possible to train models more efficiently via adversarial training alone.